Engineering the spectral profile of photon pairs by using multi-stage nonlinear interferometers

Mingyi Ma (马明毅)¹, Liang Cui (崔 亮)¹, and Xiaoying Li (李小英)*

College of Precision Instrument and Opto-Electronics Engineering, Key Laboratory of Opto-Electronics Information Technology,
Ministry of Education, Tianjin University, Tianjin 300072, People's Republic of China

¹These authors contributed equally to this work

*Corresponding author: xiaoyingli@tju.edu.cn

Received Month X, XXXX; accepted Month X, XXXX; posted online Month X, XXXX

We study the joint spectral function of photon pairs generated by nonlinear interferometers (NLIs) in which the nonlinear fibers are 2, 3 and 4 pieces, respectively. Although the photon pairs produced by single piece nonlinear fiber via four wave mixing are frequency anti-corelated, their mode profile can be flexibility modified by active filtering effect originated from the quantum interference in NLIs. We perform two series of experiments. One is that all the nonlinear fibers in pulse pumped NLIs are identical; the other is that the lengths of N pieces nonlinear fibers follow binomial distribution. We find the latter provides a better active filtering function: the separation between adjacent islands in the contour of joint spectral function increases with N, and there is no mini-maxima between two primary maxima. This feature of the uneven multi-stage NLI, which is experimentally demonstrated for the first time, is useful for efficiently engineering the factorable two-photon state—a desirable resources of quantum information processing. Our investigation shows that the multi-stage NLI is a useful tool of engineering the mode structure of quantum states.

Keywords: quantum state engineering; optical parametric amplifier; nonlinear quantum interference. doi:10.3788/COLXXXXXX.XXXXXX.

The mode structure of quantum optical fields is utmost important in quantum information processing (QIP) ^[1]. The reasons are two folds. First, many protocols in QIP, such as quantum teleportation and quantum computing, are based on quantum interference and it is crucial to have mode match between interfering fields to achieve high visibility ^[2-4]. Second, the mode profile increases the degrees of freedom for quantum fields, which brings the ability to achieve multidimensional quantum entanglement and increase the capacity of QIP ^[1,5]. Therefore, many exquisite efforts have been put on engineering the mode structure of quantum states ^[2,3,6-13].

Engineering the mode structure of quantum state by using quantum interference in SU(1,1) interferometers (NLI) has recently attracted a lot of attentions [14-21]. The SU(1,1) NLI is analogous to a conventional Mach-Zehnder interferometer but with the two beam splitters being substituted by two parametric amplifiers (PAs). It was originally proposed to achieve the Heisenberg limit in precision phase measurement [22] and had been used to demonstrate interesting applications in quantum metrology, spectroscopy and optical imaging etc. [23,24]. By using the active filtering mechanism through SU(1,1)-type nonlinear quantum interference, the mode structure of quantum states can be flexibility engineered. The quantum interferometric method realized by NLI can separate the control of mode structure from nonlinear interaction. Therefore, for the photon pairs generated from the optical parametric process, this method has the following advantages: (1) The brightness and collection efficiency of photon pairs will not be reduced since the

active filtering provided by the NLI will not reduce uncorrelated background noise photons; (2) The entire wavelength range that satisfies the phase matching condition can be used to reshaping the mode of quantum state, leading to flexibility in wavelength selection; (3) arbitrary engineering in the production of entangled photon pairs can be easily realized.

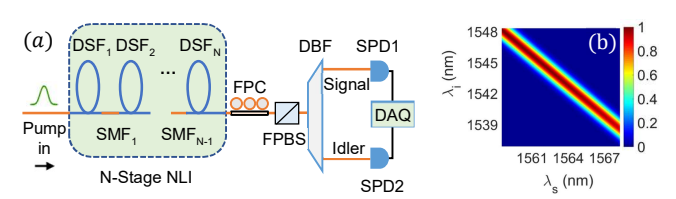


Fig. 1. (a) The experimental setup of generating photon pairs from an N-stage nonlinear interferometer (NLI), consisting of N pieces nonlinear media of dispersion shifted fibers (DSFs) and N-1 pieces phase shifters of standard single mode fibers (SMFs). DBF, dual-band filter; FPC, fiber polarization controller; FPBS, fiber polarization beam splitter; SPD, single photon detector; DAQ, data acquisition system. (b) The contour of joint spectral intensity $|F(\omega_s, \omega_i)|^2$ for photon pairs generated from single piece DSF.

The theoretical analysis and proof-in-principle experiments shows that finer mode control can be realized if the stage number of NLI (i.e., number of PAs) is greater than 2 [14,20,21]. However, most of the NLI experiments presented so far [15-19,23,24] contains of two pieces of nonlinear media. In this paper, we experimentally study the joint spectral function (JSF) of photon pairs generated from four wave mixing (FWM) in pulse pumped multi-stage NLIs,

which are formed by a sequential array of nonlinear fibers, with a gap in between made of a linear dispersive medium of standard single mode fiber. In the NLIs, the number of nonlinear fibers is up to 4 pieces. Moreover, in addition to carrying out the experiments by using NLI containing identical nonlinear fibers, we also study the performance of NLIs in which the lengths of NFs are different. Our experimental results show that the multi-stage NLI is a useful tool of engineering the mode structure of quantum states.

Our experimental setup is shown in Fig. 1. The NLI is formed by N pieces of dispersion shifted fibers (DSFs) with N-1 pieces of standard single mode fiber (SMFs) in between two adjacent DSFs. For each DSF, the zero dispersion wavelength is $\lambda_0 = 1552.5$ nm, the dispersion slope at λ_0 is $D_{slope} = 0.075 \, ps/(km \cdot nm^2)$, and the nonlinear coefficient γ is 2 $(W \cdot km)^{-1}$. When the NLI is pumped with a train of laser pulses with central wavelength of $\lambda_{p0} = 1553.3 \,\mathrm{nm}$, the phase matching condition of FWM is satisfied in each DSF. Therefore, the DSFs function as nonlinear media of FWM. On the other hand, the dispersion coefficient of standard SMF in 1550 nm band is about $D_{SMF} = 17 \ ps/(nm \cdot km)$, which is far from the satisfaction of phase matching condition, so the SMFs function as linear dispersion media, in which the precise modal control can be realized by introducing phase shift but not influencing the phase matching of FWM in DSF. The pump of NLI is obtained by passing the output of a femto-second fiber laser through a bandpass filter (F1) (see Ref. [18] for details). The full-width at half maximum (FWHM) and repetition rate of pump pulses are 1.4 nm, and 36.8 MHz, respectively. In the NLI, the transmission losses of DSFs and SMFs are negligibly small and the loss induced by each splicing point of DSF and SMF is less than 4%. In the experiments presented hereinafter, the length of each SMF, L_{DM} , is fixed at 10 m, while the number and length of DSFs can be varied.

In the spontaneous FWM process, two pump photons at ω_p scatter through the Kerr nonlinearity of DSF to create a pair of quantum correlated signal and idler photons at frequencies of ω_s and ω_i respectively. Since the spatial mode of optical fields involved in the experiment is well confined by the waveguide structure of optical fibers, we focus on analyzing the temporal mode structure of photon pairs. When the power of Gaussian shaped pump is low, the JSF of photon pairs at the output of the *N*-stage NLI can be expressed as $^{[21,24]}$:

$$F_{NLI}(\omega_s, \omega_i) = \exp\left[-\frac{(\omega_s + \omega_i - 2\omega_{p0})^2}{4\sigma_p^2}\right] \times \sum_{n=1}^{N} g_n \times e^{2i(N-1)\theta},$$
 (1)

with $g_n \propto \gamma P_p L_n \operatorname{sinc}\left(\frac{\Delta k L_n}{2}\right) \ll 1$ denoting the gain of FWM in the N-th DSF (i.e., DSF_N in Fig. 1(a)), where N is the

number of DSFs contained in the NLI, P_p and L_n are the peak pump power and length of DSF_N, $\Delta k =$ $\frac{\lambda_{p_0}^2}{8\pi c}D_{slope}(\lambda_{p0}-\lambda_0)(\omega_s-\omega_i)^2$ – $2\gamma P_p$ with c denoting the speed of light in vacuum is the phase mismatching term of FWM in DSF, $\omega_{p0}=2\pi c/\lambda_{p0}$ and σ_p are the central frequency and bandwidth of pump, and θ is the overall phase difference between pump and photon pairs of adjacent DSFs. In our experiment, the approximations $\Delta k L_n \rightarrow 0$ and sinc $\left(\frac{\Delta k L_n}{2}\right) \rightarrow 1$ hold since phase matching of FWM is satisfied in each DSF. When the internal loss in NLI is negligibly small, the gains of FWM in different pieces of DSFs can be changed by varying their lengths. Moreover, the length of each SMF is $L_{DM}=10$ m, so the amount of phase difference between pump and photon pairs introduced by each SMF, $\Delta \phi_{DM}$ is much greater than that of the term $\Delta k L_n$. Hence, in Eq. (1), we have the approximation [19,21]:

$$\theta \approx \frac{\Delta \phi_{DM}}{2} = \lambda_{p0}^2 D_{SMF} L_{DM} (\omega_s - \omega_i)^2 / 16\pi c, \qquad (2)$$

In our first experiment, the length of each DSF is 100 m, i.e., $L_1=L_2=\cdots=L_n=L=100$ m. Using the identical gain approximation $g_1=g_2=\cdots=g_n=g$, Eq. (1) has the simplified form:

$$\begin{split} F_{NLI}^{S}(\omega_{s}, \omega_{i}) &= F(\omega_{s}, \omega_{i}) \times H(\theta) \\ &= g \exp \left[-\frac{(\omega_{s} + \omega_{i} - 2\omega_{p0})^{2}}{4\sigma_{p}^{2}} \right] \operatorname{sinc}(\frac{\Delta kL}{2}) \times H(\theta), \end{split}$$
(3)

where the superscript "S" denotes that the length of each DSF in NLI is the same, $F(\omega_s, \omega_i) = g \exp\left[-\frac{(\omega_s + \omega_i - 2\omega_{p0})^2}{4\sigma_p^2}\right] \operatorname{sinc}(\frac{\Delta kL}{2})$ is the JSF of photon pairs generated by single piece DSF, and

$$H(\theta) = e^{i(N-1)\theta} \frac{\sin N\theta}{\sin \theta},\tag{4}$$

is the interference factor of the N-stage NLI. Substituting the experimental parameters of our NLI into Eqs. (2)-(4), it is straightforward to plot the contour of the interference factor $|H(\theta)|^2$ in the wavelength coordinate of λ_s and λ_i for the case of N = 2, 3, 4, as shown in Fig. 2(a). To better illustrate how the quantum interference between the photon pairs generated in different DSFs of NLI modifies the spectral property, the joint spectral intensity (JSI) of signal piece DSF is presented in Fig. 1(b), which clearly exhibits the frequency anti-correlation in the entire range of signal and idler fields satisfying the phase matching condition. One sees that the symmetry lines for contours of $|F(\omega_s, \omega_i)|^2$ in Fig. 1(b) and $|H(\theta)|^2$ are orthogonal to each other, and the contours of the *N*-stage NLI, $|F_{NLI}^S(\omega_s, \omega_i)|^2$, exhibit islands patterns, as shown in Fig. 2(b). The main maxima occur at $\theta = m\pi$ with m = 1, 2, ... being referred to as the order number. From Fig. 2(b), one sees that

depending on the stripe width of $|H(\theta)|^2$, $\sigma_{int}^2 = 4c/[(N-1)m\lambda_{p0}^2D_{SMF}L_{DM}]$, the pattern of island with specified central wavelengths changes with variations of the stage number N, order number of island m, and pump bandwidth [21]. For the photon pairs extracted from the island with specified numbers of N and m, their frequencies are anti- (positive-) correlated if the stripe width of $|H(\theta)^2|$ is $\sigma_{int} < \sqrt{2}\sigma_p$ ($\sigma_{int} > \sqrt{2}\sigma_p$), as shown by the island with N = 2 (N = 4) and M = 1 (M = 4) in Fig. 2(b). When $\sigma_{int} = \sqrt{2}\sigma_p$, the island becomes round shaped, from which the spectral factorable photon pairs can be obtained, as shown by the islands with N = 2, M = 4, and N = 3, M = 2, and N = 4, M = 1 in Fig. 2(b) [9,19,21].

To experimentally characterize the spectral profile of photon pairs, we need to extract the signal and idler photon pairs at the output of NLI. A fiber polarization controller (FPC) placed in front of the fiber polarization beam splitter (FPBS) is used to select the signal and idler photon pairs co-polarized with the pump and to reject the Raman scattering (RS) cross-polarized with the pump [26]. Because the conversion efficiency of FWM in the NLI is relatively weak, about 0.01 photon pair is produced in a single piece DSF with length of 100 m when the number of pump photons contained in a pulse of 4 ps duration is about 107. Thus, to reliably detect the correlated photon pairs, a pump to photon-pair rejection ratio in excess of 110 dB is required. We achieve this by passing the output of NLI through a dual-band filter (DBF) realized by cascading a notch filter and a programmable optical filter (POF, model: Finisar Wave shaper 4000S). For each passed band of DBF, its spectrum is rectangularly shaped, with tunable central wavelength and bandwidth.

Two superconducting nanowire single photon detectors SPD1 and SPD2 followed by a data acquisition system are utilized to count the signal and idler photons. The detection efficiencies in both signal and idler bands are about 10~% when the efficiencies of SPDs (\sim 80%) and transmission efficiency of DBF are included.

We measure the spectra of photon pairs produced by the NLI with the stage number of N = 2, 3, 4, respectively. In the experiment, the average pump power is fixed at 60 µW, the bandwidth for both the signal and idler pass bands of DBF is set to ~ 0.16 nm (0.02 THz in frequency). In addition to respectively recording the single counts of SPD1 and SPD2, we measure both the two-fold coincidence counts of signal and idler photons originated from the same pump pulse and adjacent pulses, C_c and C_{acc} , when the central wavelength of DBF in signal (idler) channel is scanned from 1558.5 nm (1548.4 nm) to 1568.3 nm (1537.9 nm) with a step of ~ 0.16 nm (0.02 THz in frequency). We then deduce the true coincidence counts of photon pairs by subtracting the measured C_{acc} from C_c . Figure 2(c) plots the contour maps of true coincidences in the wavelength coordinates of λ_s and λ_i , which reflects the JSI, $|F_{NLI}^S(\omega_s, \omega_i)|^2$, of photon pairs. We find that the contour maps of NLIs do exhibit

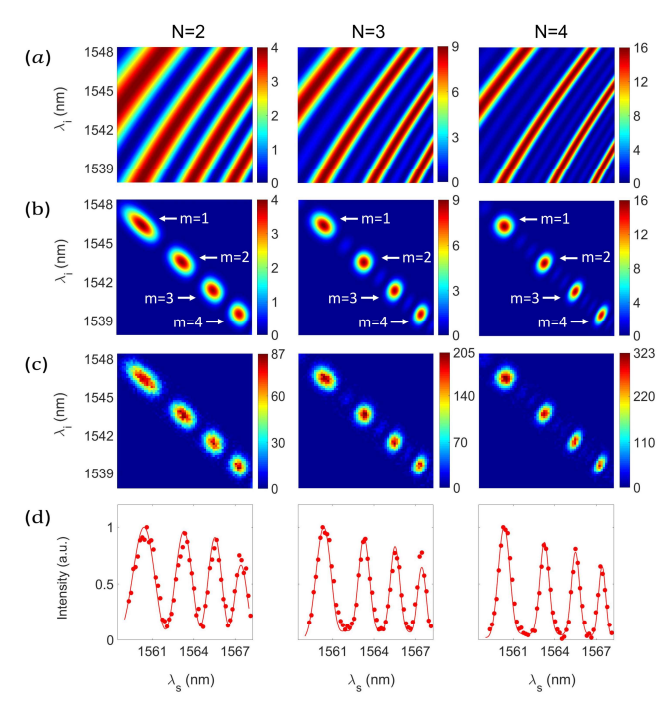


Fig. 2. The results for N-stage NLI, in which N is 2, 3, and 4, respectively, and the lengths of each DSF and SMF are 100 m and 10 m, respectively. (a) and (b) are the calculated contours of interference factor $|H(\theta)|^2$ and joint spectral intensity $|F_{NLI}^S(\omega_s,\omega_i)|^2$ in Eqs. (4) and (3), respectively. (c) Contour maps of true coincidence of photon pairs as function of λ_s and λ_i , reflecting the joint spectral intensity of photon pairs. (d) Measured (dots) and calculated (solid curves) marginal intensity distributions of signal photons. The error bars of the measurement results are within the size of data points.

islands pattern. In each plot of Fig. 2(c), the central wavelengths of the islands labelled m = 1, 2, 3, 4 in the signal (idler) band are centering at about 1560.4 nm (1546.3 nm), 1563.3 nm (1543.4 nm), 1565.5 nm (1541.3 nm), 1567.4 nm (1539.5 nm), respectively. The results indicate that the central wavelengths of the islands do not vary with N. For the NLI with a fixed stage number N, the distance between the maxima of adjacent primary islands decreases with the increase of detuning $(\lambda_s - \lambda_i)$; moreover, the width of the island decreases with the order number m. This is because the phase shift θ in Eq. (2) quadratically depends on the detuning of photon pairs ($\omega_s - \omega_i =$ $-2\pi c(\lambda_s - \lambda_i)/\lambda_{n_0}^2$, and the width of $|H(\theta)|^2$ decreases with the increase of m. On the other hand, for the island with a fixed order number m, the width of the island decreases with the increase of N. Moreover, the counting rates corresponding to the highest peaks of the primary islands are 87±5, 205±10 and 323±18 counts/s when the integration time spent in taking each data point is 3, 2, and 1 second for N = 2, 3, 4, respectively. Comparing with the rate measured from 100 m long single piece DSF, the peak intensity for the measured true coincidences of the NLI increases with N and the increasement agree with the scale of N^2 predicted in Eq. (4). In the cases of N > 3, there exists

N-2 secondary islands between two adjacent primary islands. The counting rates for all the peaks of the secondary islands are around 20-30 counts/s. So the ratio between the intensities of the primary and secondary islands increases with the increase of N. The comparison of Figs. 2(c) and 2(b) shows that the experimental results well agree with the theoretical predictions.

In the meantime of characterizing JSF, the marginal intensity distribution in individual signal and idler fields can be respectively acquired from the counting rates of SPD1 and SPD2. Because the data of the two fields is similar, for the sake of brevity, we only present the results in signal field. Fig. 2(d) shows the normalized rate of single counts (via FWM) as a function of the wavelength in signal channel. Each plot in Fig. 2(d) exhibits interference pattern, illustrating the NLI functions as an active filter of photon pairs. In order to clearly visualize the active filter function, the data (dots) in Fig. 2(d) is obtained after correcting the Raman effect [26]. We find the measurement well agree with the theoretically calculated results (solid curves). It is clear that the periodicity of interference pattern in the three plots of Fig. 2(d) is the same since the phase shifters in each case are identical. For the interference fringes with a fixed peak wavelength, which are originated from the islands with same order number m, the fringe width decreases with the increase of N due to the increased separation of adjacent islands in JSF; while the visibility of the interference fringe, defined by $V_m = (I_{max}^m - I_{min}^m)/I_{max}^m$ with I_{max}^m and I_{min}^m respectively denoting the normalized intensity at the peak and trough, increases with N. One sees that V_m takes the lowest value for the case of N=2due to the existence of overlap of between two adjacent islands. However, even if N is large, the minimum of the normalized intensity (single count rates) I_{min}^m is still away from 0 due to the secondary islands existed in between two adjacent primary islands. Note that in the process of selecting the photon pairs with spectral profile determined by one specific island, the filter bandwidth should be properly set to fully pick out one island and to isolate adjacent islands as much as possible [19]. So the collection efficiency of photon pairs, characterized by the probability of detecting the photon at signal (idler) band for a photon detected in the idler (signal) band, is closely related to interference fringe presented in marginal intensity distribution. To improve the collection efficiency, the visibility of the corresponding fringe in Fig. 2(d) should be as high as possible. The non-ideal visibility (less than 1) will prevent the collection efficiency of photon pairs from reaching the ideal value of 1, in particular, when the NLI is designed to engineer the factorable state $^{[18,19,21]}$.

Further analysis reveals that the secondary islands in between adjacent primary islands of JSF originate from the H-function in Eq. (4), which normally gives (N-1)-th harmonic of $\cos 2\theta$, i.e., $\cos 2(N-1)\theta$. It is possible to get rid of the mini-maxima of secondary islands by using uneven length DSF for different part of the N-stage NLI.

When the linear dispersion media of SMFs still have the same length but the lengths of DSFs are arranged by using binomial distribution

$$L_n = L_1 C_{N-1}^{n-1} = L_1 \frac{(N-1)!}{(n-1)!(N-n)!},$$
 (5)

 $F_{NLI}(\omega_s, \omega_i)$ in Eq. (1) has the simplified form

$$F_{NLI}^{(UN)}(\omega_s, \omega_i) \approx \exp\left[-\frac{(\omega_s + \omega_i - 2\omega_{p0})^2}{4\sigma_p^2}\right] \times K(\theta),$$
 (6)

with the interference factor given by

$$K(\theta) = \sum_{n=1}^{N} L_n e^{2i(n-1)\theta} = L_1 (1 + e^{2i\theta})^{N-1}, \quad (7)$$

where the superscript "UN" refers to the NLI with uneven length DSFs, θ is the same as in Eq. (2). Therefore, if the different sections of NLI follow a binomial pattern, e.g., $L_1\colon L_2\colon L_3=1:2:1$ for N=3 and $L_1\colon L_2\colon L_3\colon L_4=1:3:3:1$ for N=4, we then have $|K(\theta)|^2=L_1^{-2}4^{(N-1)}\cos^{N-1}(2\theta)$. There is no mini-maxima in $|K(\theta)|^2$. Figure 3(a) shows the contours of the interference factor $|K(\theta)|^2/L_1^{-2}$ for the cases of N=3,4, respectively. It is clear that the variation tendency of $|K(\theta)|^2/L_1^{-2}$ is similar to that in Fig. 2(a),

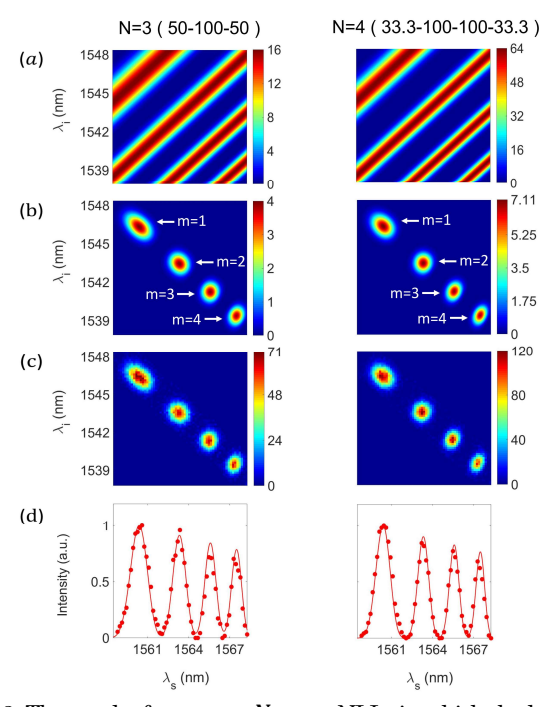


Fig. 3. The results for uneven N-stage NLIs, in which the lengths of DSFs, labelled in the top for different stage number N, follow binomial distribution and the length of each SMF is 10 m. (a, b) The calculated contours of interference factor $|K(\theta)|^2/(L_1^2)$ and joint spectral intensity $|F_{NLI}^{(UN)}(\omega_s,\omega_i)|^2$ (see Eqs. (6) and (7)), respectively. (c) Contour maps of true coincidence of photon pairs as function of λ_s and λ_i , reflecting the joint spectral intensity of photon pairs. (d) Measured (dots) and calculated (solid curves) marginal intensity distributions of signal photons.

except that the mini-maxima does not exist anymore. The width of the main maxima still narrows as N increases, leading to enlarged islands separation in JSF (see Fig. 3(a)).

We then perform the second experiment to verify the spectral profile of uneven N-stage NLI for the cases of N =3, 4, respectively. In the experiment, the parameters are the same as that in Fig. 2, except for the arrangement of DSFs follows binomial distribution (see Eq. (5)). When N =3, the lengths of three DSFs, L_1 , L_2 , and L_3 are 50, 100 and 50 m, respectively; when N = 4, the lengths of four DSFs, L_1 , L_2 , L_3 and L_4 , are 33.3, 100, 100, and 33.3 m, respectively. Figure 3(c) shows the contour maps of true coincidences in the wavelength coordinates of signal and idler, λ_s and λ_i . The counting rates corresponding to the highest peaks of the islands are 71±3 and 114±5 counts/s for N = 3.4, respectively. The centers of islands and the variation tendencies of the islands are the same as those of N=3 and N=4 cases in Fig. 2. The separation between two adjacent islands increases with N, but the secondary islands do not exist anymore. Comparing Fig. 3(c) with Fig. 3(b), in which the results are calculated by substituting the experimental parameters into Eq. (6), we find the measured islands patterns of JSI well agree with theory predictions.

Moreover, we characterize the active filter function of the uneven N-stage NLI by deducing the marginal intensity distribution in individual signal and idler fields. The results in two fields are similar. Fig. 3(d) shows the data (dots) in signal channel, which is obtained after correcting the Raman effect ^[26]. We find the data agree with the theoretically calculated results (solid curves). Comparing with Fig. 2(d), One sees that for the NLI with same stage number of N, the visibility of interference fringes in Fig. 3(d) is higher.

It's well known that the spectral factorable photon pairs with high collection efficiency are the desirable resources of quantum information processing. Recent investigation shows that the quantum interference in NLI provide an alternative approach for achieving this kind of photon pairs^[19-21]. So, we pay more attention on round shaped islands, from which the spectral factorable state can be obtained without sacrificing collection efficiency. For the round islands in Fig. 2, obtained under the condition of (i) N = 2, m = 4, (ii) N = 3, m = 2, and (iii) N = 4, m = 1, the visibility in Fig. 2(d) is obviously deviate from the ideal results of 1 due to the existence of overlap (N = 2) or the min-maxima (N > 3). While for both the cases of (ii) N = 3, m=2 and (iii) N=4, m=1 in Fig. 3, the fringe visibilities of the round island in Fig. 3(d) are approaching to the ideal value of 1 because of the increased separation and the elimination of mini-maxima. This analysis and comparison indicate that if the NLIs are used to engineering factorable state, higher collection efficiency of photon pairs can be obtained by the properly designed uneven NLI with N > 3.

Finally, although the RS accompanying the FWM in DSFs can be significantly suppressed by cooling the fibers [18,19,27], we would like to point out that our experiments are conducted at room temperature. This is because the goal of the paper is to reveal the role of multi-stage NLI played in modifying the spectral profile of photon pairs, which is characterized by the JSF. Cooling fiber will add unnecessary complexity. When the pass bands of DBF are scanned, at each wavelength setting, we measure the counting rates $R_{s(i)}$ in individual signal (idler) channel at different levels of average pump power P_a and then fit the measured data with a second-order polynomial $R_{s(i)}$ = $s_1P_a + s_2P_a^2$, where s_1 and s_2 are the fitting parameters. The linear and quadratic terms, s_1P_a and $s_2P_a^2$, are respectively proportional to the intensities of RS and FWM. The data points plotted in Figs. 2(d) and 3(d) are obtained by subtracting the portion RS photons from the raw data $R_{s(i)}$. Figure 4 shows two typical sets of raw data obtained at the wavelengths of 1560.4 nm and 1561.9 nm, which respectively correspond to the peak and valley of N=4case in Fig. 2(d). We find that comparing with the quadratic part (dotted curve) in Fig. 4(a), the quadratic term in Fig. 4(b) is negligibly small due to the interference effect. When pump power is fixed at 60 µW, the ratio between the quadratic terms in Figs 4(a) and 4(b) is 16.3, indicating the visibility of the fringe is about 94%, which is in consistent with the theoretical prediction of 95.7%.

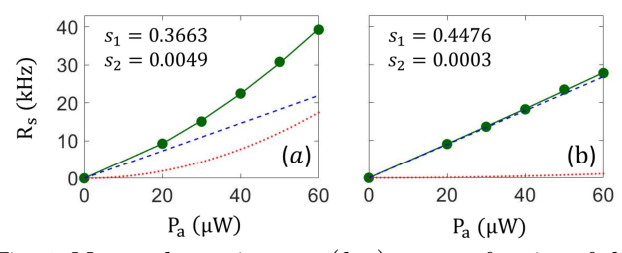


Fig. 4. Measured counting rate (dots) R_s as a function of the average pump power P_a for signal photons at (a) 1560.44 nm and (b) 1561.9 nm, respectively. The solid curves $R_s = s_1 P_a + s_2 P_a^2$ are the fitting function of raw data (dots), dashed and dotted lines are the linear term $s_1 P_a$ and quadratic term $s_2 P_a^2$, respectively.

In conclusion, we experimentally investigate the spectral pumped multi-stage pulse interferometers, formed by an array of DSFs with a standard SMF placed in between two adjacent DSFs. In the experiment, the number of DSFs is N = 2, 3, 4, respectively. We perform two series of experiments. One is that all the DSFs in NLI are identical; the other is that the lengths of the DSFs follow binomial distribution. The experimental results well agree with theoretical predictions. Moreover, we find the uneven multi-stage NLI provides a better active filtering function: the separation between adjacent islands in the contour of joint spectral function increases with N, and there is no mini-maxima between two primary maxima. To the best of our knowledge, this is the first experimental demonstration of uneven multi-stage NLI. This feature of the uneven multi-stage NLI is useful for efficiently engineering the factorable two-photon state, from which the pure state single photons with high efficiency, high brightness and high flexibility in wavelength and bandwidth selection can be obtained. Our investigation illustrates that although the photon pairs produced by single piece DSF via four wave mixing are frequency anti-corelated, their mode profile can be flexibility modified by active filtering effect originated from the quantum interference in N-stage NLI, and the NLI with stage number greater than 2 has more flexibility in modifying the mode structure of quantum state.

This work was supported by the National Natural Science Foundation of China (11527808, 11874279), and Science and Technology Program of Tianjin (18ZXZNGX00210).

References

- C. Fabre and N. Treps, http://www.arxiv.org/abs/1912.0932
 1v1 (December 19, 2019) (to appear in Rev. Mod. Phys).
- J. Pan, D. Bouwmeester, W. Harald, and Z. Anton, Phys. Rev. Lett. 80, 3891 (1998).
- D. Bouwmeester, J. Pan, M. Klaus, E. Manfred, W. Harald, and Z. Anton, Nature 390, 575 (1997).
- E. Knill, R. Laflamme, and G. J. Milburn, Nature 409, 46 (2001).
- B. Brecht, Dileep V. Reddy, C. Silberhorn, and M. G. Raymer, Phys. Rev. X 5, 041017 (2015)
- 6. Z. Y. Ou, Quantum Semiclass. Opt. 9, 599 (1997).
- 7. W. P. Grice and I. A. Walmsley, Phys. Rev. A 56, 1627 (1997).
- P. J. Mosley, J. S. Lundeen, B. J. Smith, P. Wasylczyk, A. B. U' Ren, C. Silberhorn, and I. A. Walmsley, Phys. Rev. Lett. 100, 133601 (2008).
- K. Garay-Palmett, H. J. McGuinness, O. Cohen, J. S. Lundeen, R. Rangel-Rojo, A. B. U'Ren, M. G. Raymer, C. J. McKinstrie, S. Radic, and I. A. Walmsley, Opt. Express 15, 14870 (2007).
- O. Cohen, J. S. Lundeen, B. J. Smith, G. Puentes, P. J. Mosley, and I. A. Walmsley, Phys. Rev. Lett. 102, 123603 (2009).
- 11. L. Cui, X. Li, and N. Zhao, New. J. Phys. 14, 123001 (2012).
- P. G. Evans, R. S. Bennink, W. P. Grice, T. S. Humble, and J. Schaake, Phys. Rev. Lett. 105, 253601 (2010).
- A. M. Brańczyk, A. Fedrizzi, T. M. Stace, T. C. Ralph, and A. G. White, Opt. Express 19, 55 (2011).
- A. B. U'Ren, C. Silberhorn, K. Banaszek, I. A. Walmsley, R. Erdmann, W. P. Grice, and M. G. Raymer, Laser Phys. 15, 146 (2005).
- G. Frascella, E. E. Mikhailov, N. Takanashi, R. V. Zakharov, O. V. Tikhonova, and M. V. Chekhova, Optica 6, 1233 (2019).
- G. Frascella, R. V. Zakharov, O. V. Tikhonova, and M. V. Chekhova, Laser Phys. 29, 124013 (2019).
- S. Lemieux, M. Manceau, P. R. Sharapova, O. V. Tikhonova, R. W. Boyd, G. Leuchs, and M. V. Chekhova, Phys. Rev. Lett. 117, 183601 (2016).
- J. Su, L. Cui, J. Li, Y. Liu, X. Li, and Z. Y. Ou, Opt. Express 27, 20479 (2019).
- J. Li, J. Su, L. Cui, T. Xie, Z. Y. Ou, and X. Li, Appl. Phys. Lett. 116, 204002 (2020).

- N. Huo, Y. Liu, J. Li, L. Cui, X. Chen, R. Palivela, T. Xie, X. Li, and Z. Y. Ou, Phys. Rev. Lett. 124, 213603 (2020).
- L. Cui, J. Su, J. Li, Y. Liu, X. Li, and Z. Y. Ou, http://www.arxiv.org/abs/1811.07646v2 (April 20, 2020) (to appear in Phys. Rev. A).
- B. Yurke, S. L. McCall, and J. R. Klauder, Phys. Rev. A 33, 4033 (1986).
- M. V. Chekhova and Z. Y. Ou, Adv. Opt. Photonics 8, 104 (2016).
- Z. Y. Ou and Xiaoying Li, http://www.arxiv.org/abs/2004.124
 69v1 (April 26, 2020) (to appear in APL photonics.)
- D. A. Kalashnikov, A. V. Paterova, S. P. Kulik, and L. A. Krivitsky, Nat. Photonics 10, 98 (2016).
- X. Li, J. Chen, P. Voss, J. E. Sharping, and P. Kumar, Opt. Express 12, 3737 (2004).
- S. D. Dyer, B. Baek, and S. W. Nam, Opt. Express 17, 10290– 10297 (2009)

References

- C. Fabre and N. Treps, "Modes and states in quantum optics," http://www.arxiv.org/abs/1912.09321v1 (December 19,2019) (to appear in Rev. Mod. Phys).
- 2. J. Pan, D. Bouwmeester, W. Harald, and Z. Anton, "Experimental entanglement swapping: entangling photons that never interacted", Phys. Rev. Lett. 80, 3891 (1998).
- D. Bouwmeester, J. Pan, M. Klaus, E. Manfred, W. Harald, and Z. Anton, "Experimental quantum teleportation", Nature 390, 575 (1997).
- E. Knill, R. Laflamme, and G. J. Milburn, "A scheme for efficient quantum computation with linear optics," Nature 409, 46 (2001).
- B. Brecht, Dileep V. Reddy, C. Silberhorn, and M. G. Raymer, "Photon temporal modes: A complete framework for quantum information science", Phys. Rev. X 5, 041017 (2015)
- Z. Y. Ou, "Parametric down-conversion with coherent pulse pumping and quantum interference between independent fields", Quantum Semiclass. Opt. 9, 599 (1997).
- W. P. Grice and I. A. Walmsley, "Spectral information and distinguishability in type-II down-conversion with a broadband pump", Phys. Rev. A 56, 1627 (1997).
- 8. P. J. Mosley, J. S. Lundeen, B. J. Smith, P. Wasylczyk, A. B. U' Ren, C. Silberhorn, and I. A. Walmsley, "Heralded generation of ultrafast single photons in pure quantum states", Phys. Rev. Lett. 100, 133601 (2008).
- K. Garay-Palmett, H. J. McGuinness, O. Cohen, J. S. Lundeen, R. Rangel-Rojo, A. B. U'Ren, M. G. Raymer, C. J. McKinstrie, S. Radic, and I. A. Walmsley, "Photon pair-state preparation with tailored spectral properties by spontaneous four-wave mixing in photonic-crystal fiber", Opt. Express 15, 14870 (2007).
- O. Cohen, J. S. Lundeen, B. J. Smith, G. Puentes, P. J. Mosley, and I. A. Walmsley, "Generation of uncorrelated photon-pairs in an optical fiber", Phys. Rev. Lett. 102, 123603 (2009).
- L. Cui, X. Li, and N. Zhao, "Minimizing the frequency correlation of photon pairs in photonic crystal fibers", New. J. Phys. 14, 123001 (2012).
- P. G. Evans, R. S. Bennink, W. P. Grice, T. S. Humble, and J. Schaake, "Bright source of spectrally uncorrelated polarization-entangled photons with nearly single-mode emission", Phys. Rev. Lett. 105, 253601 (2010).
- 13. A. M. Brańczyk, A. Fedrizzi, T. M. Stace, T. C. Ralph, and A. G. White, "Engineered optical nonlinearity for quantum light sources", Opt. Express 19, 55 (2011).
- A. B. U'Ren, C. Silberhorn, K. Banaszek, I. A. Walmsley, R. Erdmann, W. P. Grice, and M. G. Raymer, "Generation of pure-state single-photon wave packets by conditional preparation based on spontaneous parametiric down conversion", Laser Phys. 15, 146 (2005).
- G. Frascella, E. E. Mikhailov, N. Takanashi, R. V. Zakharov,
 O. V. Tikhonova, and M. V. Chekhova, "Wide-field SU(1,1) interferometer", Optica 6, 1233 (2019).
- G. Frascella, R. V. Zakharov, O. V. Tikhonova, and M. V. Chekhova, "Experimental reconstruction of spatial Schmidt

- modes for a wide-field SU(1,1) interferometer", Laser Phys. 29, 124013 (2019).
- S. Lemieux, M. Manceau, P. R. Sharapova, O. V. Tikhonova, R. W. Boyd, G. Leuchs, and M. V. Chekhova, "Engineering the frequency spectrum of bright squeezed vacuum via group velocity dispersion in an SU(1,1) interferometer", Phys. Rev. Lett. 117, 183601 (2016).
- J. Su, L. Cui, J. Li, Y. Liu, X. Li, and Z. Y. Ou, "Versatile and precise quantum state engineering by using nonlinear interferometers," Opt. Express 27, 20479 (2019).
- J. Li, J. Su, L. Cui, T. Xie, Z. Y. Ou, and X. Li, "Generation of pure-state single photons with high heralding efficiency by using a three-stage nonlinear interferometer," Appl. Phys. Lett. 116, 204002 (2020).
- N. Huo, Y. Liu, J. Li, L. Cui, X. Chen, R. Palivela, T. Xie, X. Li, and Z. Y. Ou, "Direct temporal mode measurement for the characterization of temporally multiplexed high dimensional quantum entanglement in continuous variables", Phys. Rev. Lett. 124, 213603 (2020).
- 21. L. Cui, J. Su, J. Li, Y. Liu, X. Li, and Z. Y. Ou, "Quantum state engineering by nonlinear quantum interference", http://www.arxiv.org/abs/1811.07646v2 (April 20, 2020) (to appear in Phys. Rev. A).
- B. Yurke, S. L. McCall, and J. R. Klauder, "SU(2) and SU(1,1) interferometers", Phys. Rev. A 33, 4033 (1986).
- M. V. Chekhova and Z. Y. Ou, "Nonlinear interferometers in quantum optics", Adv. Opt. Photonics 8, 104 (2016).
- 24. Z. Y. Ou and Xiaoying Li, "Quantum Entangled Interferometers." http://www.arxiv.org/abs/2004.12469v1 (April 26, 2020) (to appear in APL photonics).
- D. A. Kalashnikov, A. V. Paterova, S. P. Kulik, and L. A. Krivitsky, "Infrared spectroscopy with visible light", Nat. Photonics 10, 98 (2016).
- X. Li, J. Chen, P. Voss, J. E. Sharping, and P. Kumar, "All-fiber photon-pair source for quantum communications: Improved generation of correlated photons", Opt. Express 12, 3737 (2004).
- S. D. Dyer, B. Baek, and S. W. Nam, "High-brightness, lownoise, all-fiber photon pair source", Opt. Express 17, 10290– 10297 (2009)